Exchange bias training in $La_{0.7}Sr_{0.3}FeO_3/Ni_{79}Fe_{21}$ films with native surface oxide: First-order reversal curve analysis

Z. W. Liang,[1,2] Z.-H. Wang,[2,*] B.-G. Shen,[2] L. C. Wang,[2] F. P. Wang,[1] and P. Wu[1]

[1]*Department of Physics, University of Science and Technology Beijing, Beijing 100083, China*

[2]*Beijing National Laboratory for Condensed Matter Physics and State Key Laboratory for Magnetism, Institute of Physics, Chinese Academy of Sciences, Beijing 100190, China*

(Received 1 October 2020; revised 16 July 2021; accepted 9 August 2021; published 24 August 2021; corrected 9 September 2021)

In conventional magnetometry, exchange bias training (EBT) is mostly evaluated through the major magnetization hysteresis loops (MHLs). We here report a study of EBT by using the first-order reversal curves (FORCs) in the heterostructures of $SrTiO_3(001)/La_{0.7}Sr_{0.3}FeO_3$(LSFO)$/Ni_{79}Fe_{21}(Py)/PyO_x$. It was unraveled that the training effect occurs once after exceeding the left coercivity of the first MHL, while the magnetic coupling from the ultrathin native oxide (PyO_x) mainly contributes to an exchange springlike behavior. Besides for the first MHL, the FORCs corresponding to the second MHL and the quasiequilibrium stage were collected, respectively, which provide a detailed picture of how the magnetization reversal evolves in the training process.

DOI: 10.1103/PhysRevB.104.064440

I. INTRODUCTION

Exchange bias is associated with an exchange coupling phenomenon between antiferromagnetic (AF) and ferromagnetic (FM) materials [1]. As an emergent magnetic property, it plays an active role in modern passive spintronic devices [2–4]. Experimentally, the major magnetization hysteresis loop (MHL) displays a horizontal shift (H_{eb}) and a loop width (H_c) broadening in occurrence of exchange bias. Nevertheless, both the $H_{eb,c}$ tend to decay with cycling the magnetic field (H). This training effect has so far been explained by several different models, such as the rearrangement of AF spin structure towards equilibrium [5,6], the symmetry driven irreversibility under inherent spin frustration [7,8], and the domain wall formation parallel or perpendicular to the AF/FM interface [9–12]. In spite of all these efforts, its physical basis is still under debate.

A comprehensive understanding of exchange bias training requires an insight into the AF instability. This now relies heavily on the measurements on large-scale facilities, like neutron diffraction [13,14] and synchrotron-based x-ray linear dichroism [15]. It is thus advantageous to probe the subtle evolution relevant to the AF instability by using the general laboratory tools. As for using magnetometry, the minor first order reversal curves (FORCs) have recently attracted increasing attention [16], because of the extra information they could offer on magnetization reversal in comparison with the major MHLs [17]. In analogy with the Preisach modeling [18,19], the FORC measurements are usually implemented as follows: After saturating the positive magnetization, the magnetic field is decreased to a reversal field (H_r), from which a single FORC of $M(H, H_r)$ is traced out by measuring the partial (minor) loop as the field is swept back towards the positive saturation; A family of FORCs can be constituted through repeating the measurements but with a series of H_rs till the negative saturation. The corresponding FORC distribution (ρ) is defined as

$$\rho(H, H_r) = -\frac{1}{2}\frac{\partial^2 M(H, H_r)}{\partial H_r \partial H}, \tag{1}$$

where the preset negative sign before the mixed derivative reflects the fact that all the H_rs locate on the descending branch of the MHL. According to this definition, the nonzero ρ characterizes the irreversible switching processes, therefore enabling a quantitative measure of the local exchange interactions and distributions, which are not readily extracted from the major MHLs. The FORC study has been performed for diverse magnetic systems, such as single layers [20], multilayers [21–24], exchange spring films [25,26], patterned structures [27–33], graded composites [34,35], permanent magnets [36,37], and phase separated oxides [38]. The FORC analysis have been also employed for investigating exchange bias, but where the training effect was either left unaddressed [39–42], or claimed to be absent [31], or intentionally removed by field cycling for a great number of times before the FORC measurement [43].

In such a context, we here report a FORC study of exchange bias training in the films of $La_{0.7}Sr_{0.3}FeO_3$(LSFO)$/Ni_{79}Fe_{21}$(Py)$/PyO_x$. The Py with the Curie temperature of ~830 K [44], is a prototypical soft FM material exploited in exchange biased units [2]. The bottom oxide LSFO owns a G-type AF structure with a Néel temperature of about 360 K [45–48]. According to the finite-size scaling theory [49–51], the critical temperature for the AF transition in the ultrathin native oxide (PyO_x) is estimated to be ~184–235 K [52]. It is also noteworthy that, except for the conventional AF/FM systems based on CoO, NiO and Fe_2O_3 [1,2], the metal-oxide heterostructures for studying exchange bias are hitherto still limited.

*Author to whom correspondence should be addressed: z.wang@iphy.ac.cn

II. EXPERIMENTAL DETAILS

The sample in an initial stacking of $SrTiO_3$ (STO)(001)/LSFO(350)/Py(12)/Ag(5) was grown in a multisource sputtering facility [53], and below it is referred to as the exchange biased film. Meanwhile, the reference film without LSFO was prepared in a stacking of STO(001)/Py(12)/Ag(5). The nominal thicknesses in brackets here and below are in units of nanometers. The deposition rates were calibrated through growing thick film for each material, and measuring the thickness by using scanning electron microscopy (Hitachi S-4800). Specifically, the LSFO films were grown by radio frequency (rf) sputtering onto single crystal STO(001) substrate at 800 °C. The target source with a 2-in. diameter was tilted about 42° away from the film normal direction. The rf sputtering was run at a power of 60 W, a base pressure of 4.3×10^{-5} Pa, and a gas pressure of 2.0 Pa (Ar : $O_2 \sim 19 : 1$). After the rf sputtering, the LSFO films were *in situ* annealed at 850 °C for 1 h and then cooled in oxygen under pressure of 50 Pa. The polycrystalline Py film was deposited onto LSFO or bare STO(001) substrate by direct current (dc) sputtering at ambient temperature. The dc sputtering was performed at a power of 60 W, a base pressure of 2.1×10^{-5} Pa and an Ar pressure of 0.3 Pa. At last, the Ag cap layer was deposited onto the Py film by dc sputtering. The films were kept in a desiccator in ambient air pressure when they were not in measurements. The issue of the ultrathin native oxidation (PyO_x) for both the exchange biased and the reference films will be addressed later in light of the MHL measurements.

The x-ray diffraction was carried out on a Bruker x-ray diffractometer (D8 Advanced) with Cu $K\alpha$ radiation. The film surface morphology was characterized by using scanning probe microscopy (Seiko SPI3800N). The MHL and FORCs were measured using a Quantum Design superconducting quantum interference device (SQUID) vibrating sample magnetometer (VSM). The remanent magnetic field (−0.5 to −4.6 Oe) from the superconductor magnet was corrected by monitoring the center for the MHL of a standard sample in palladium foil, just before and/or after the magnetic measurements. In this work, a family of FORCs comprises 100 partial (minor) reversal curves, which were all measured in a field spacing of 20 Oe and a field sweep rate of 50 Oe/s. The smooth factor SF = 2 was taken for displaying the contour of the FORC diagrams.

III. RESULTS AND DISCUSSION

Figure 1(a) shows the atomic force image of the LSFO film. The film surface morphology exhibits a coherent granular feature with the root-mean-square (rms) roughness of about 1.27 nm (Fig. S1, Supplemental Material [52]). Figure 1(b) displays the $\theta \sim 2\theta$ x-ray diffraction pattern of the exchange biased film. In accordance with the epitaxial growth reported on STO(001) [54–56], the LSFO film shows only the (00l) peak adjacent to the similar reflection of the substrate. The derived out-of-plane lattice constant $c_{\mathrm{LSFO}} \sim 3.971$ Å. In terms of a pseudocubic symmetry, the lattice constant for bulk LSFO (a_p) is about 3.896 Å [57]. The LSFO film grown on the cubic STO ($a_s = 3.905$ Å) is accordingly imposed with a strain of

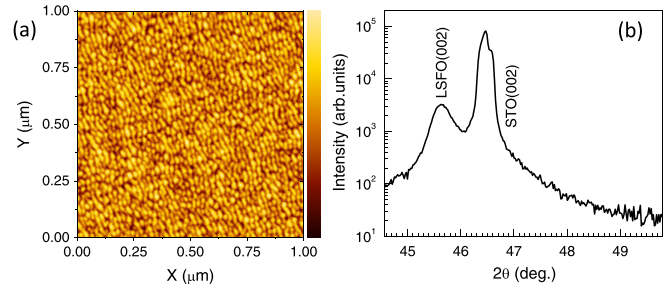

FIG. 1. (a) The atomic force image of the LSFO film surface morphology, for which the color bar for height ranges 0–8 nm. (b) The $\theta \sim 2\theta$ x-ray diffraction pattern for the LSFO/Py/PyO_x film grown onto STO(001).

$(a_s - a_p)/a_s \sim +0.2\%$. This slight tensile strain should have been relaxed in the present LSFO film with a large thickness of 350 nm. The elongated c_{LSFO} would be consequently resulted from a chemical expansion effect due to the oxygen vacancies infiltrated during the film growth [58,59].

Generally, exchange bias training becomes pronounced with decreasing temperature. The MHLs of the exchange biased film were thus measured at 2 K, close to the lower bound of 1.8 K for the SQUID-VSM. Figure 2(a) shows the MHLs measured continuously only through increasing the loop numbers (n) after a +1 kOe field cooling (FC, along [100]) from 400 K. In the first MHL ($n = 1$), the demagnetization process leads to a magnetization kink at about −120 Oe, as shown by a closeup view and a plot of dM/dH vs H [Fig. 2(b) and its inset]; furthermore, the main magnetic switchings occur at the left coercive field ($H_c^{\mathrm{left}} \sim -653$ Oe) and the right

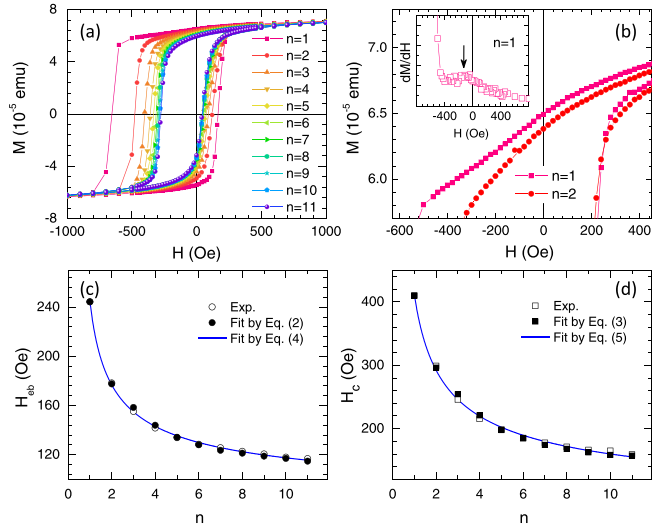

FIG. 2. (a) The magnetization hysteresis loops (MHLs) for the exchange biased film of LSFO(350)/Py(8)/PyO_x(4) measured at 2 K after the field cooling with $H_{\mathrm{FC}} = +1$ kOe along [100] from 400 K. (b) The MHLs ($n = 1$ and 2) shown in the first and second quadrants indicate the low field magnetization kink only with $n = 1$ at about −120 Oe, which is confirmed by the inset plot of dM/dH vs H for the descending branch of the first MHL. (c), (d) The exchange bias field H_{eb} (c) and coercive field H_c (d) as function of n, in which the data fits ($n \geqslant 1$) are based on Eqs. (2)–(5).

TABLE I. Parameters for fitting $H_{eb}(n)$ and $H_c(n)$ ($n \geqslant 1$) shown in Figs. 2(c) and 2(d) by using Eqs. (2)–(5). R^2 characterizes the goodness of fit.

Parameters	Fit of $H_{eb}(n)$	Fit of $H_c(n)$
	by Eq. (2)	by Eq. (3)
$H_{eb,c}(\infty)$ (Oe)	45.51 ± 6.23	-4.30 ± 17.97
$\gamma_{eb,c}(10^{-6}$ Oe$^{-2})$	8.50 ± 0.91	1.60 ± 0.24
R^2	0.991 04	0.989 31
	by Eq. (4)	by Eq. (5)
$H_{eb,c}(\infty)$ (Oe)	77.62 ± 1.64	62.36 ± 6.88
$k_{eb,c}$ (Oe)	123.22 ± 3.98	305.35 ± 17.86
$n_{eb,c}$	-0.46 ± 0.03	-0.23 ± 0.07
R^2	0.999 21	0.997 47

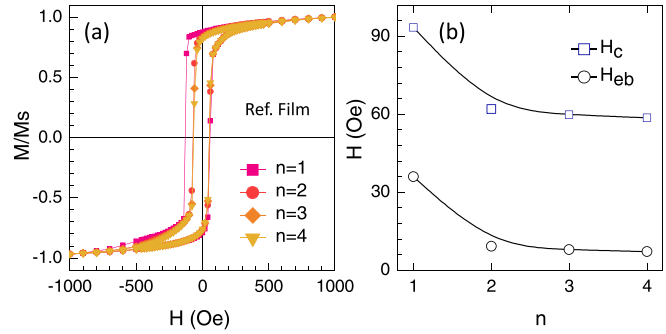

FIG. 3. (a) The MHLs for the reference film of STO/Py/PyO$_x$ measured at 2 K after the field cooling with $H_{FC} = +1$ kOe along [100] from 400 K. (b) The derived H_{eb} and H_c shown as function of n.

coercive field ($H_c^{right} \sim 167$ Oe), respectively, indicating an exchange bias field $H_{eb} = -(H_c^{left} + H_c^{right})/2 \approx 243$ Oe and $H_c = (H_c^{right} - H_c^{left})/2 \approx 410$ Oe. Upon cycling the fields, the low field magnetization kink becomes hardly distinguishable from $n = 2$ [Fig. 2(b)], while the training process with n up to 11 reveals a monotonic decrease in both $H_{eb,c}$ [Figs. 2(c) and 2(d)].

For a simulation of the training effect, we attempt to employ the recursive relation

$$H_{eb}(n+1) - H_{eb}(n) = -\gamma_{eb}[H_{eb}(n) - H_{eb}(\infty)]^3, \quad (2)$$

proposed by Binek [5], where γ is a system dependent constant, and $H_{eb}(\infty)$ represents an equilibrium value. As shown in Fig. 2(c), Eq. (2) can well fit the data ($n \geqslant 1$) with positive γ and $H_{eb}(\infty)$ (see Table I). We find that if extending this relation to $H_c(n)$,

$$H_c(n+1) - H_c(n) = -\gamma_c[H_c(n) - H_c(\infty)]^3, \quad (3)$$

Eq. (3) can simulate the data but yields a negative $H_c(\infty)$ of large variance [Fig. 2(d) and Table I]. In fact, a better fit with positive $H_c(\infty)$ can be achieved by excluding the data with $n = 1$ (Fig. S2 in the Supplemental Material [52]). To quest a common relation for describing both the $H_{eb,c}(n)$ ($n \geqslant 1$), we next adopt the modified power-law (MPL) [60–62], which is similar to the empirical $1/\sqrt{n}$ dependence [63],

$$H_{eb}(n) = H_{eb}(\infty) + k_{eb}(n + n_{eb})^{-1/2}, \quad (4)$$

$$H_c(n) = H_c(\infty) + k_c(n + n_c)^{-1/2}, \quad (5)$$

where $k_{eb;c}$ are system dependent, and $n_{eb;c}$ are dimensionless. As illustrated in Figs. 2(c) and 2(d) and Table I, one can see that Eqs. (4) and (5) allow good fits with reasonable $H_{eb,c}(\infty)$.

For a comparison, the MHLs of the reference film were also measured at 2 K after the FC. Unexpectedly, as shown in Figs. 3(a) and 3(b), the first MHL ($n = 1$) exhibits a loop shift ($H_{eb} = 35$ Oe) and an $H_c = 93$ Oe which is much higher than the coercivity ($H_c < 10$ Oe) at the similar low temperature for the Py ultrathin films grown onto nonmagnetic substrate [64,65]. Upon field cycling, the training effect occurs, but soon tends to be stabilized at $n = 4$ with $H_c \sim 58$ Oe and $H_{eb} \sim 6$ Oe. In the absence of LSFO, this loop shift with an H_c enhancement indicates an AF component, most likely arising from the native surface oxide PyO$_x$ [51,66]. Due to the same growth condition, this Py surface oxidation should also occur in the above exchanged biased film. Note that the granular surface morphology of the LSFO film can be readily transferred to the Py layer. Because of the high interfacial energy of Ag, the surface roughness of the upper Ag capping layer can be enhanced, which possibly enables pinholes and then allows oxygen diffusion into the Py layer [51,67,68].

If assuming a magnetic moment of 8.6×10^5 A m^{-1} for Py [69], the PyO$_x$ thickness of ~4 nm can be known from the decreased magnetization saturation (M_s) shown in Fig. 2(a). This reveals a stacking of LSFO(350)/Py(8)/PyO$_x$(4) for the exchange biased film. Compared to the $H_{eb,c}$ of the reference film, the relative increment in H_{eb} is much higher than in H_c for the exchange biased film, suggesting that the exchange anisotropy in the latter film should be primarily controlled by the LSFO film. On the other hand, the low field magnetization kink shown in the MHL can be ascribed to the weaker coupling at the Py/PyO$_x$ interface, which should contribute largely to the H_c because of the ultrathin AF (PyO$_x$) layer [2], and may thus explain why the recursive relation of Eq. (3) leads to an unsatisfactory fit for the $H_c(n)$ data from $n = 1$. In contrast, Eqs. (4) and (5) allowing good fits can be attributed to the fact that the MPL model in principle considers an *overall* evolution of the nonequilibrium AF configurations in the system.

A preliminary FORC study for the exchange biased film starts as follows: After the FC to 2 K, two families of FORCs (Λ_1, Λ_2) were *consecutively* collected, i.e., the last reversal curve of the FORC-Λ_1 was directly followed by the first reversal curve of the FORC-Λ_2. In Figs. 4(a) and 4(d), we show the FORCs and the typical MHLs ($n = 1$, 2, and 11) replotted from Fig. 2(a). In the FORC-Λ_1 [Fig. 4(a)], the descending magnetization envelope including the low field magnetization kink coincides with the descending branch of the first MHL (Fig. S3 in the Supplemental Material [52]). However, a clear disparity exists between the FORCs and the ascending branch of the first MHL. The closeup view unveils that the FORCs with $H_r = -660$ to -680 Oe set the right outermost frontier of the FORC-Λ_1, and upon increasing H_r to negative saturation, the FORC abnormally moves inwards and becomes stabilized at the ascending branch of the MHL with $n = 11$ [Fig. 4(b)]. It implies that the training effect occurs just after the very first magnetic switching when

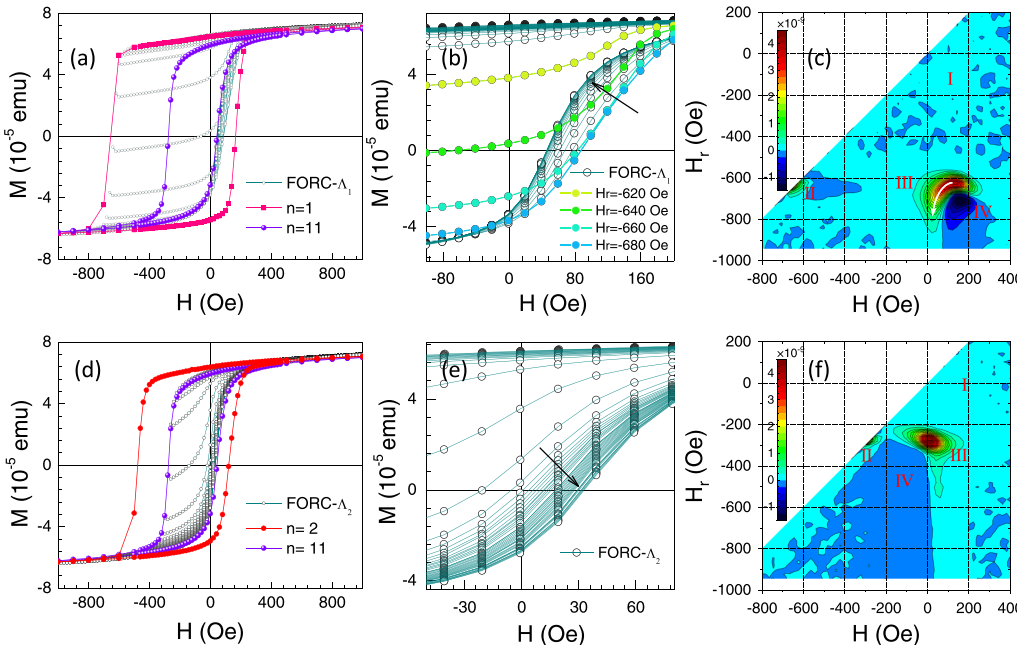

FIG. 4. FORC study of the exchange biased film of LSFO(350)/Py(8)/PyO$_x$(4): (a) The families of FORC-Λ_1 compared to the MHLs with $n = 1$ and 11 [replotted from Fig. 2(a)]. (b) The closeup view of the right outmost frontier of the FORC-Λ_1, in which the FORCs with $H_r = -620$ to -680 Oe (close to the $H_c^{\text{left}} \approx -653$ Oe for the first MHL) are again individually plotted in progressive colors, and the arrow indicates the abnormal inward moving. (c) The FORC-Λ_1 diagram, where the typical regions are denoted by I–IV, and the bending feature in the positive ridge is indicated by a curved arrow. (d) The families of FORC-Λ_2 compared to the MHLs with $n = 2$ and 11 [replotted from Fig. 2(a)]. (e) The closeup view of the right outmost frontier of the FORC-Λ_2. The arrow indicates the monotonic outward expanding. (f) The FORC-Λ_2 diagram.

$|H - H_c^{\text{left}}(n = 1)| > 17$ Oe. In the FORC-Λ_2 [Fig. 4(d)], the reversal curves monotonically expand with H_r [Fig. 4(e)], and in the end, *both* the left descending envelope and the right outermost FORC nearly coincide with the 11th rather than the second MHL, showing that this family of FORCs is close to probing a well trained state.

The corresponding FORC-$\Lambda_{1,2}$ distributions are displayed in Figs. 4(c) and 4(f), respectively. In the FORC-Λ_1 diagram, four regions (I–IV) are noteworthy. Region I of no appreciable features ($\rho \approx 0$) is derived from the nearly overlapped FORCs with -580 Oe $< H_r < 200$ Oe. The descending envelope of these reversal curves in fact reenacts the low field magnetization kink in the first MHL, thus implying that the associated coupling at the upper interface (Py/PyO$_x$) should mainly result in an exchange springlike process which corresponds to a reversible magnetization reversal. Region II shows a positive peak at about the axis of local bias field [$h_b = (H + H_r)/2$] with $H_r \sim H_c^{\text{left}}(n = 1) \sim -653$ Oe. In connection with the field sweeping rate, this edge peak signifies the onset of the irreversible magnetic switching [70,71]. At the bottom right of the diagram, the neighboring regions III and IV are prominent. The positive distribution (region III) is similar in appearance to a boomerang with tip rightward. This is in contrast to the case in nonexchange biased systems where the FORC distribution is also in the shape of a boomerang but with tip leftward [24,29,36]. Here, the ridge along the H axis is associated with confined H_rs around -653 Oe, indicating a rapid nucleation of reversed magnetic domains near the $H_c^{\text{left}}(n = 1)$; As denoted by a curved arrow, the ridge in bending to the lower left corresponds to the reversal curves that move inward while yielding a larger slope of $\partial M/\partial H$ with increasing H_r, thus intuitively showing the emergence of training effect in the FORC measurements. In region IV, the negative distribution presents with the deepest valley at $(H, H_r) \sim (158, -710)$ Oe which is rather close to the positive peak at $\sim(100, -620)$ Oe. This distribution is also associated with the FORCs that abnormally move inward, but more directly corresponds to the FORCs with the upper magnetic fields, where the slope of $\partial M/\partial H$ decreases with increasing H_r [72]. In both regions III and IV, the local FORC distributions in a form of peak-valley pair extend up to $H_r \sim -850$ Oe, indicating persistent domain annihilations even beyond a perceived magnetic saturation [21,34].

In the FORC-Λ_2 diagram, the relevant regions I–IV change as below: Region I of $\rho \approx 0$ is reduced to -200 Oe $\leqslant H_r \leqslant$ 200 Oe. The edge peak in region II moves to $H_r = -276$ Oe which is close to the H_c^{left} for the MHL with $n = 11$. The positive distribution in region III becomes mostly centered around $(H, H_r) \sim (4, -276)$ Oe, while the ridgelike profile is somewhat off the H axis. The prior pair of positive-negative feature leaves a trace, but in which the positive distribution now fades away along the vertical ridge (-580 Oe $\leqslant H_r \leqslant -380$ Oe), while the negative valley becomes shallow and extended. These features suggest that the magnetization reversal for the well trained state should be dominated by incoherent spin rotation rather than by domain nucleation and annihilation.

The above FORCs (Λ_1 and Λ_2) are informative, however, they miss detecting the training stage at $n = 2$, which in fact displays a marked difference from the case with $n = 1$ [Figs. 2(a)–2(d)], as known also from the data fit results using

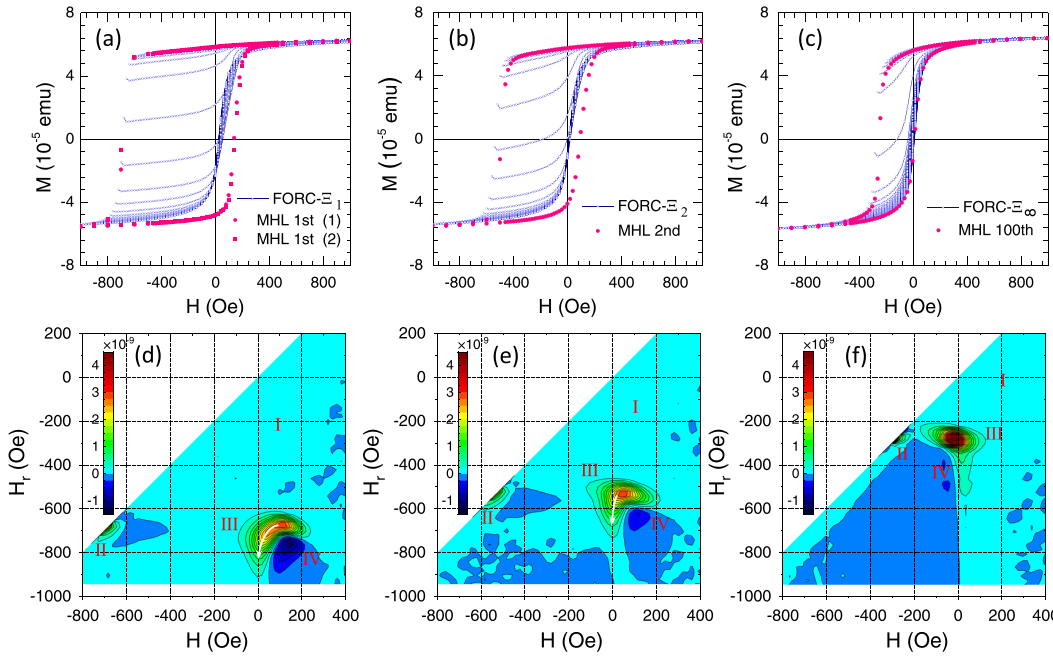

FIG. 5. The FORCs and diagrams for the exchange biased film of LSFO(350)/Py(7)/PyO$_x$(5): FORC-Ξ_1 (a), (d), FORC-Ξ_2 (b), (e), and FORC-Ξ_∞ (c), (f). The MHLs ($n = 1$, 2, and 100) newly measured in between, are shown in (a)–(c), respectively. Note that the two MHLs with $n = 1$ (a) were measured in two independent runs, i.e., each was measured after a +1 kOe field cooling from 400 K. The bending features in the positive ridge in (d) and (e) are indicated by a curved arrow (d) and a less curved arrow (e), respectively.

Eq. (3) (Fig. S2 in the Supplemental Material [52]). To seek an intuitive picture of the evolution, three new families of FORCs (Ξ_1, Ξ_2, Ξ_∞) were measured at 2 K respectively by following a procedure as below: After the FC to 2 K, the FORC-Ξ_1 corresponding to the first MHL was measured as before; after one more FC to 2 K and measuring the first MHL, the FORC-Ξ_2 corresponding to the second MHL was measured; again FC from 400 to 2 K, but then after measuring the MHLs with n up to 100, the FORC-Ξ_∞ was measured, corresponding to the quasiequilibrium stage of little training effect.

Figure 5 shows the FORCs [Ξ_1(a), Ξ_2(b), Ξ_∞(c)] with the derived diagrams [(d)–(f)], and also the MHLs ($n = 1$, 2, and 100) newly measured in between. It should be noted that all these measurements were performed two months later since the prior measurements for the FORC-$\Lambda_{1,2}$ and the relevant MHLs ($n = 1$–11). Owing to the time span, the native surface oxidation in the exchange biased film should develop a bit further. As evaluated from the M_s shown in Fig. 5(a), the stacking configuration for the exchange biased film now evolves into LSFO(350)/Py(7)/PyO$_x$(5). The newly obtained $H_{\rm eb} \sim 270$ Oe ($n = 1$) was larger than the prior one ($\sim$243 Oe), also indicating a slight reduction in the Py thickness (t_{FM}) through the relation of $H_{\rm eb} \propto 1/t_{\rm FM}$ [2]. In line with the prior observation, however, the descending envelope of the FORC-Ξ_1 matches the descending branch of the new MHL with $n = 1$, which shows a low field magnetization kink also at ~ -120 Oe (Fig. S4 in the Supplemental Material [52]) and a nearly unchanged $H_c \sim 415$ Oe. Furthermore, both the FORCs and diagrams (Ξ_1 and Ξ_∞) are very similar to the cases of the FORC-Λ_1 and -Λ_2, respectively. For instance, the inward moving of the reversal curves with H_r exceeding the first $H_c^{\rm left}$ [Figs. 5(a) and 6(b)], the positive-negative pair of features, and the bending feature in the FORC-Ξ_1 diagram due to the training effect [Fig. 5(d)], the monotonic outward expanding with H_r in the FORC-Ξ_∞, and its right outermost frontier matching the the ascending branch of the 100th MHL [Figs. 5(c) and 6(f)]. All the consistencies confirm our above analysis, while also indicating that (i) the slight further oxidation in Py does not markedly affect the exchange coupling at the Py/PyO$_x$ interface, and (ii) the prior film after the 11th MHLs should have already been in a quasiequilibrium state.

For the FORC-Ξ_2, its right outermost frontier does not match the ascending branch of the new MHL with $n = 2$ [Fig. 5(b)], as expected from the referred training effect. Unlike both the cases in the FORC-Λ_1 and the FORC-Ξ_1, however, the descending envelope of the FORC-Ξ_2 was found to move leftward ($\sim$60 Oe) with respect to the descending branch of the second MHL [see also Fig. 6(c)]. For the FORC-Ξ_∞, its descending envelope was also found to move left about 40 Oe, compared to the descending branch of the 100th MHL [Figs. 5(c) and 6(e)]. After the MHL with $n = 100$, the system should have reached a quasiequilibrium state with little training effect. The enhancement in the left coercive field for the descending envelopes of the FORCs (Ξ_2, Ξ_∞) would imply a slight regain of the initial AF configuration by the positive magnetic saturations, when the H_r is smaller than the $H_c^{\rm left}$ of the corresponding MHL.

In comparison with the FORC-Ξ_1, the abnormal inward moving for the FORC-Ξ_2 shows in a more slender region [Figs. 5(b) and 6(d)]. In the FORC-Ξ_2 diagram [Fig. 5(e)], the positive distribution in region III is now similar in appearance

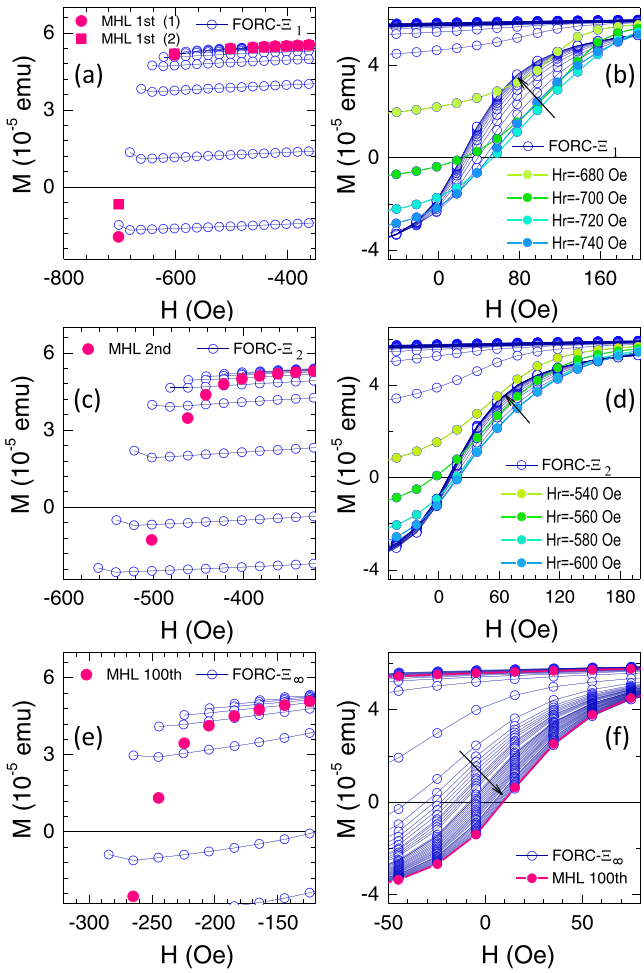

FIG. 6. The closeup views for the FORCs (Ξ_1, Ξ_2, and Ξ_∞) shown in Figs. 5(a)– 5(c) with H_rs around the H_c^{left} of the corresponding MHL [Ξ_1 (a), Ξ_2 (c), and Ξ_∞ (e)], and around the right outmost frontier [Ξ_1 (b), Ξ_2 (d), and Ξ_∞ (f)]. Like in Fig. 4(b), the FORCs with $H_r = -680$ to -740 Oe in (b) and with $H_r = -540$ to -600 Oe in (d) are again individually plotted in progressive colors. The arrows indicate the abnormal inward moving (b), (d) and the monotonic outward expanding (f).

to a deformed boomerang. Compared to the FORC-Ξ_1 diagram, the bending feature due to the training effect (indicated by a less curved arrow) as well as the negative distribution in the peak-valley pair (starting from $H_r \sim -600$ Oe) appears less pronounced. Meanwhile, the positive peak is more centered on the ridge and discernibly off the H axis, which becomes somewhat similar to the FORC-Ξ_∞ diagram. It implies that the irreversible switching of the MHL with $n = 2$ still mainly involves domain nucleation and annihilation, however, which should be incorporated with some incoherent spin rotations. It also clearly shows that the FORC measurements are indeed able to reflect a subtle evolution in the training process, even though the outermost envelopes of the reversal curves are not exactly matching the major MHL.

IV. CONCLUSION

In summary, we have exploited the FORCs to study the training effect in the exchange biased heterostructures of STO/LSFO/Py/PyO$_x$. We find that the FORCs and the derived diagrams can give quantitative measures of the magnetic couplings due to the AF/FM interfaces, the early occurrence of the train effect, and how the magnetization reversal mode in the training process evolves from domain nucleation and annihilation to incoherent spin rotation. Our work demonstrates the FORC analysis as a simple yet valuable approach for investigating exchange bias coupling and reversal process, because of its inherent sensitivity to irreversible magnetic switching.

ACKNOWLEDGMENTS

This work was supported by the Science Center of the National Science Foundation of China under Grant No. 52088101, the National Natural Science Foundation of China under Grants No. 11474342 and No. 11174353, the National Key Research and Development Program of China, and the Strategic Priority Research Program B of the Chinese Academy of Sciences. Z.-H.W. acknowledges the support from F. X. Hu, M. Hu, J. H. Yin, and S. L. He.

[1] W. H. Meiklejohn and C. P. Bean, Phys. Rev. **105**, 904 (1957).
[2] J. Nogués and I. K. Schuller, J. Magn. Magn. Mater. **192**, 203 (1999); A. E. Berkowitz and K. Takano, *ibid.* **200**, 552 (1999).
[3] T. Jungwirth, X. Marti, P. Wadley, and J. Wunderlich, Nat. Nanotechnol. **11**, 231 (2016).
[4] V. Baltz, A. Manchon, M. Tsoi, T. Moriyama, T. Ono, and Y. Tserkovnyak, Rev. Mod. Phys. **90**, 015005 (2018).
[5] Ch. Binek, Phys. Rev. B **70**, 014421 (2004).
[6] W. Echtenkamp and Ch. Binek, Phys. Rev. Lett. **111**, 187204 (2013).
[7] A. Hoffmann, Phys. Rev. Lett. **93**, 097203 (2004).
[8] S. Brems, K. Temst, and C. Van Haesendonck, Phys. Rev. Lett. **99**, 067201 (2007).
[9] D. Suess, M. Kirschner, T. Schrefl, J. Fidler, R. L. Stamps, and J.-V. Kim, Phys. Rev. B **67**, 054419 (2003).
[10] F. Radu, M. Etzkorn, R. Siebrecht, T. Schmitte, K. Westerholt, and H. Zabel, Phys. Rev. B **67**, 134409 (2003).
[11] S. Brems, D. Buntinx, K. Temst, C. Van Haesendonck, F. Radu, and H. Zabel, Phys. Rev. Lett. **95**, 157202 (2005).
[12] T. Hauet, J. A. Borchers, Ph. Mangin, Y. Henry, and S. Mangin, Phys. Rev. Lett. **96**, 067207 (2006).
[13] A. Paul and A. Teichert, Appl. Phys. Lett. **97**, 032505 (2010).
[14] E. Menéndez, T. Dias, J. Geshev, J. F. Lopez-Barbera, J. Nogués, R. Steitz, B. J. Kirby, J. A. Borchers, L. M. C. Pereira, A. Vantomme, and K. Temst, Phys. Rev. B **89**, 144407 (2014).
[15] A. N. Dobrynin, F. Maccherozzi, S. S. Dhesi, R. Fan, P. Bencok, and P. Steadman, Appl. Phys. Lett. **105**, 032407 (2014).
[16] C. Pike, A. Roberts, and K. Verosub, J. Appl. Phys. **85**, 6660 (1999).

[17] G. Bertotti, *Hysteresis in Magnetism* (Academic, San Diego, 1998).

[18] I. Mayergoyz, IEEE Trans. Magn. **MAG-22**, 603 (1986).

[19] I. Mayergoyz, *Mathematical Models of Hysteresis* (Springer-Verlag, New York, 1991).

[20] D. Navas, N. Soriano, F. Béron, C. T. Sousa, K. R. Pirota, J. Torrejon, C. Redondo, R. Morales, and C. A. Ross, Phys. Rev. B **96**, 180403(R) (2017).

[21] J. E. Davies, O. Hellwig, E. E. Fullerton, G. Denbeaux, J. B. Kortright, and K. Liu, Phys. Rev. B **70**, 224434 (2004).

[22] J. E. Davies, O. Hellwig, E. E. Fullerton, and K. Liu, Phys. Rev. B **77**, 014421 (2008).

[23] J. E. Davies, O. Hellwig, E. E. Fullerton, M. Winklhofer, R. D. Shull, and K. Liu, Appl. Phys. Lett. **95**, 022505 (2009).

[24] J. H. Yin, H.-W. Zhang, F. X. Hu, B.-G. Shen, and L. Q. Pan, J. Appl. Phys. **106**, 103901 (2009).

[25] J. E. Davies, O. Hellwig, E. E. Fullerton, J. S. Jiang, S. D. Bader, G. T. Zimányi, and K. Liu, Appl. Phys. Lett. **86**, 262503 (2005).

[26] H.-C. Hou, B. J. Kirby, K. Z. Gao, and C.-H. Lai, Appl. Phys. Lett. **102**, 162408 (2013).

[27] C. Pike and A. Fernandez, J. Appl. Phys. **85**, 6668 (1999).

[28] C. R. Pike, C. A. Ross, R. T. Scalettar, and G. Zimanyi, Phys. Rev. B **71**, 134407 (2005).

[29] M. T. Rahman, R. K. Dumas, N. Eibagi, N. N. Shams, Y.-C. Wu, K. Liu, and C.-H. Lai, Appl. Phys. Lett. **94**, 042507 (2009).

[30] R. K. Dumas, C.-P. Li, I. V. Roshchin, I. K. Schuller, and K. Liu, Phys. Rev. B **75**, 134405 (2007).

[31] R. K. Dumas, C.-P. Li, I. V. Roshchin, I. K. Schuller, and K. Liu, Phys. Rev. B **86**, 144410 (2012).

[32] A. Rotaru, J.-H. Lim, D. Lenormand, A. Diaconu, J. B. Wiley, P. Postolache, A. Stancu, and L. Spinu, Phys. Rev. B **84**, 134431 (2011).

[33] F. Groß, S. E. Ilse, G. Schütz, J. Gräfe, and E. Goering, Phys. Rev. B **99**, 064401 (2019).

[34] V. Bonanni, Y. Fang, R. K. Dumas, C. Zha, S. Bonetti, J. Nogués, and J. Åkerman, Appl. Phys. Lett. **97**, 202501 (2010).

[35] Y. Fang, R. K. Dumas, T. N. Anh Nguyen, S. M. Mohseni, S. Chung, C. W. Miller, and J. Åkerman, Adv. Funct. Mater. **23**, 1919 (2013).

[36] T. Schrefl, T. Shoji, M. Winklhofer, H. Oezelt, M. Yano, and G. Zimanyi, J. Appl. Phys. **111**, 07A728 (2012).

[37] S. Okamoto, K. Miyazawa, T. Yomogita, N. Kikuchi, O. Kitakami, K. Toyoki, D. Billington, Y. Kotani, T. Nakamura, T. Sasaki, T. Ohkubo, K. Hono, Y. Takada, T. Sato, Y. Kaneko, and A. Kato, Acta Mater. **178**, 90 (2019).

[38] J. E. Davies, J. Wu, C. Leighton, and K. Liu, Phys. Rev. B **72**, 134419 (2005).

[39] J. Olamit, K. Liu, Z.-P. Li, and I. K. Schuller, Appl. Phys. Lett. **90**, 032510 (2007).

[40] L. Alonso, T. R. F. Peixoto, and D. R. Cornejo, J. Phys. D: Appl. Phys. **43**, 465001 (2010).

[41] M. Kaur, W. Jiang, Y. Qiang, E. C. Burks, K. Liu, F. Namavar, and J. S. McCloy, J. Appl. Phys. **116**, 173902 (2014).

[42] R. A. Gallardo, S. Khanal, J. M. Vargas, L. Spinu, C. A. Ross, and C. Garcia, J. Phys. D: Appl. Phys. **50**, 075002 (2017).

[43] R. Wu, J. Z. Wei, X. L. Peng, J. B. Fu, S. Q. Liu, Y. Zhang, Y. H. Xia, C. S. Wang, Y. C. Yang, and J. B. Yang, Appl. Phys. Lett. **104**, 182403 (2014).

[44] B. D. Cullity and C. D. Graham, *Introduction to Magnetic Materials*, 2nd ed. (Wiley, Hoboken, NJ, 2009), Chap. 13.

[45] J.-C. Grenier, N. Ea, M. Pouchard, and M. M. Abou-Sekkina, Mater. Res. Bull. **19**, 1301 (1984).

[46] U. Shimony and J. M. Knudsen, Phys. Rev. **144**, 361 (1966).

[47] Y. Jia, R. V. Chopdekar, E. Arenholz, Z. Liu, M. D. Biegalski, Z. D. Porter, A. Mehta, and Y. Takamura, Phys. Rev. B **93**, 104403 (2016).

[48] M. S. Lee, P. Lyu, R. V. Chopdekar, A. Scholl, S. T. Retterer, and Y. Takamura, J. Appl. Phys. **127**, 203901 (2020).

[49] R. Zhang and R. F. Willis, Phys. Rev. Lett. **86**, 2665 (2001).

[50] X. Y. Lang, W. T. Zheng, and Q. Jiang, Phys. Rev. B **73**, 224444 (2006).

[51] L. Frangou, G. Forestier, S. Auffret, S. Gambarelli, and V. Baltz, Phys. Rev. B **95**, 054416 (2017).

[52] See Supplemental Material at http://link.aps.org/supplemental/10.1103/PhysRevB.104.064440 for details of the critical temperature estimation, the sample characterization, the $H_c(n)$ data fit, and the low field magnetization kink seen in the MHLs and the descending envelope of the FORCs, which includes Refs. [49–51].

[53] Z. W. Liang, Z.-H. Wang, Y. Feng, Q. H. Zhang, L. C. Wang, C. Wang, L. Gu, P. Wu, and B.-G. Shen, Phys. Rev. B **99**, 064304 (2019).

[54] Y. Takamura, F. Yang, N. Kemik, E. Arenholz, M. D. Biegalski, and H. M. Christen, Phys. Rev. B **80**, 180417(R) (2009).

[55] E. Arenholz, G. van der Laan, F. Yang, N. Kemik, M. D. Biegalski, H. M. Christen, and Y. Takamura, Appl. Phys. Lett. **94**, 072503 (2009).

[56] L. Wang, Y. Du, P. V. Sushko, M. E. Bowden, K. A. Stoerzinger, S. M. Heald, M. D. Scafetta, T. C. Kaspar, and S. A. Chambers, Phys. Rev. Materials **3**, 025401 (2019).

[57] Bulk LSFO shows an orthorhombic (*Pbnm*, $a_o = 5.4952$ Å, $b_o = 5.5212$ Å, $c_o = 7.7953$ Å) and/or a rhombohedral phase ($R\bar{3}c$, $a_h = 5.5276$ Å, $c_h = 13.4212$ Å). Hence, if in terms of a pseudocubic unit cell, $a_p \sim 3.8964$ Å. See O. Clemens, M. Kuhn, and R. Haberkorn, J. Solid State Chem. **184**, 2870 (2011).

[58] U. Aschauer, R. Pfenninger, S. M. Selbach, T. Grande, and N. A. Spaldin, Phys. Rev. B **88**, 054111 (2013).

[59] Z.-H. Wang, Q. H. Zhang, G. Gregori, G. Cristiani, Y. Yang, X. Li, L. Gu, J. R. Sun, B.-G. Shen, and H.-U. Habermeier, Phys. Rev. Materials **2**, 054412 (2018).

[60] Y. Su and J. Hu, J. Appl. Phys. **112**, 043906 (2012).

[61] W.-B. Rui, M.-C. He, B. You, Z. Shi, S.-M. Zhou, M.-W. Xiao, Y. Gao, W. Zhang, L. Sun, and J. Du, Chin. Phys. B **23**, 107502 (2014).

[62] Z.-H. Wang, G. Cristiani, H.-U. Habermeier, and B.-G. Shen, Appl. Phys. Lett. **115**, 243501 (2019).

[63] D. Paccard, C. Schlenker, O. Massenet, R. Montmory, and A. Yelon, Phys. Status Solidi B **16**, 301 (1966).

[64] C. Hou, H. Fujiwara, T. J. Klemmer, R. M. Metzger, and W. D. Doyle, IEEE Trans. Magn. **33**, 3625 (1997).

[65] Y. S. Jung and O. S. Song, J. Korean Mag. Soc. **14**, 163 (2004).

[66] H. Ouyang, K.-W. Lin, C.-C. Liu, S.-C. Lo, Y.-M. Tzeng, Z.-Y. Guo, and J. van Lierop, Phys. Rev. Lett. **98**, 097204 (2007).

[67] G. Mihajlović, D. K. Schreiber, Y. Liu, J. E. Pearson, S. D. Bader, A. K. Petford-Long, and A. Hoffmann, Appl. Phys. Lett. **97**, 112502 (2010).

[68] B. L. Zink, M. Manno, L. O'Brien, J. Lotze, M. Weiler, D. Bassett, S. J. Mason, S. T. B. Goennenwein, M. Johnson, and C. Leighton, Phys. Rev. B **93**, 184401 (2016).

[69] M. Donahue and D. G. Porter, OOMMF Users Guide, Version 1.0, NIST Interagency Report No. 6376 (National Institute of Standards and Technology, Gaithersburg, MD, 1999).

[70] P. Andrei, O. Caltun, and A. Stancu, Phys. B (Amsterdam, Neth.) **372**, 265 (2006).

[71] D. R. Cornejo, R. D. Noce, T. R. F. Peixoto, N. Barelli, P. T. A. Sumodjo, and A. V. Benedetti, J. Alloys Compd. **479**, 43 (2009).

[72] A. Muxworthy, D. Heslop, and W. Williams, Geophys. J. Int. **158**, 888 (2004).

Correction: The wrong subscript to Ξ for the (b),(e) panels in the caption to Figure 5 was presented and has been fixed.